ACS Catalysis

Research Article

pubs.acs.org/acscatalysis

Composition-Dependent Performance of $Ce_xZr_{1-x}O_2$ Mixed-Oxide-Supported WO_3 Catalysts for the NO_x Storage Reduction−Selective Catalytic Reduction Coupled Process

Fabien Can,* Sébastien Berland, Sébastien Royer, Xavier Courtois, and Daniel Duprez

Université de Poitiers, CNRS UMR 7285, IC2MP, 4 Rue Michel Brunet, Bât. B27, 86022 Poitiers Cedex, France

ABSTRACT: $WO_3/Ce_xZr_{1-x}O_2$ materials were evaluated as a possible NH_3-selective catalytic reduction (SCR) active catalyst in a NO_x storage reduction (NSR) + SCR combined system. The effect of the support composition was investigated at a constant WO_3 loading (9.1 wt % of WO_3). The impact of WO_3 promotion over textural, structural, acid−base, and redox properties of SCR samples was characterized by means of nitrogen adsorption−desorption isotherms, XRD, NO_x storage capacity, NH_3 temperature programmed desorption, pyridine adsorption followed by FTIR, and H_2-TPR. Catalytic activities in NH_3-SCR and NH_3-SCO reactions as well as corresponding kinetics parameters are also discussed. All $WO_3/Ce-Zr$ materials are active and fully selective in N_2 for NO_x reduction by NH_3 and ammonia oxidation by O_2. For the SCR reaction, the rate of NO conversion is found approximately half-order with respect to NO, and negative to nearly zero-order with respect to NH_3. Tungstated ceria−zirconia materials were then associated downstream with a model Pt−Ba/Al NSR catalyst. Whatever the WO_3−Ce/Zr catalyst, the global NO_x conversion and N_2 yield are significantly enhanced by the addition of the SCR catalyst. Special attention is paid to the influence of the ceria content of the SCR catalyst on the ammonia reactivity in the combined NSR + SCR system. It is demonstrated that NH_3 produced during the regeneration step of Pt−Ba/Al catalyst can react either with NO_x (NH_3-SCR) or with O_2 (NH_3-SCO). This reactivity depends both on the Ce/Zr ratio of support and on the temperature. Finally, it is demonstrated that at high temperature (i.e., 400 °C), the strength of the acid sites of the WO_3−Ce/Zr catalysts is not sufficient to ensure no ammonia slip.

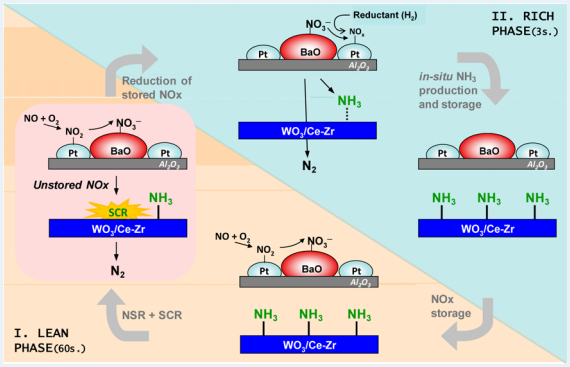

KEYWORDS: *NO_x, NH_3, SCR, NSR, tungsten, $WO_3/Ce_xZr_{1-x}O_2$*

1. INTRODUCTION

Regulations on passenger car emissions focus on the continuous minimization of NO_x emission in automotive exhaust gases, particularly for those issued from lean combustion, thast is, in an excess of air. Among the various technologies developed to reduce NO_x from diesel and lean-burn engines, the NO_x storage reduction (NSR) or lean NO_x trap (LNT)[1] and the selective catalytic reduction (SCR) are the two most studied technologies.

The NSR process works mainly in lean conditions. NO_x compounds are then oxidized on the precious metal phase and stored on basic compounds, mainly as nitrate species. Periodically, the catalyst is submitted to rich conditions for a few seconds, which allows the desorption and the reduction of stored NO_x into N_2 on the precious metal phase. Among the disadvantages of this system, the selectivity of the reduction can be problematic, with the possible emission of NH_3 and N_2O, a powerful greenhouse gas. In addition, NSR catalysts present some limitations with possible thermal deactivation, sulfur poisoning and limited deNO_x efficiency.[2,3]

The selective catalytic reduction remains as an attractive way to reduce NO_x in an excess of O_2, with the use of a large choice of reductants such as hydrocarbons (HC),[4−12] urea, ammonia,[13−15] hydrogen, alcohol,[16,17] etc. Although HC-SCR was largely studied, urea-SCR is accepted as exhibiting the highest potential to reduce NO_x emissions from heavy-duty diesel engines. In addition, it presents the advantage of possibly being added downstream to a NSR catalyst to maximize the global NO_x abatement and the N_2 selectivity, together with the prevention of the ammonia slip.[18] Ammonia produced during the brief period of regeneration of the NSR catalyst can be stored on the second SCR catalytic bed. Stored NH_3 can thereafter react with NO_x passing through the NO_x trap during the lean period via the NH_3-SCR reaction.

The concept of adding a NH_3 adsorbing materials to a NO_x reduction catalyst was first patented by Toyota in 1998 for applications on gasoline engines.[19,20] Since then, Toyota has upgraded their process to give increases recently to several systems associated with NSR and SCR catalysts.[21,22] In 2002, Daimler-Chrysler claimed a system that includes an ammonia-generating catalyst coupled with the NO_x trap or a three-way catalyst.[23] In 2004, Ford[24,25] patents claimed a NSR catalyst composed of noble metals deposited on NO_x trap materials

Received: December 20, 2012
Revised: February 21, 2013
Published: April 2, 2013

(alkali, alkali earth metals, etc.) while the SCR catalyst would be made of zeolite, or oxide-supported catalysts, as silica−alumina or titania promoted by Cu, Fe, or Ce. The coupling between a NSR and a SCR catalyst was also claimed by Engelhardt[26] or BASF.[27−29] In a patent,[27] the claimed SCR catalyst is composed of silver tungstate, Ag_2WO_4, supported on alumina. A NSR−SCR coupling system was also depicted by Johnsson-Matthey,[30] and Eaton Corporation.[31−36]

In most practical applications, the NSR + SCR system is composed of a usual NSR material in association with metal-exchanged zeolite or acidic oxides as the SCR sample. The SCR catalyst has to present both acid sites to stored ammonia emitted from the regeneration step of the NSR sample and high activity for NO_x reduction by NH_3, with reaction pathways of the NH_3-SCR described by eqs 1−4. These reactions are usually denoted as "standard" (eq 1), "fast" (eq 2), "NO_2-SCR" (eq 3), and "slow" (eq 4) SCR reactions.[13,37−41]

$$4NH_3 + 4NO + O_2 \rightarrow 4N_2 + 6H_2O \quad (1)$$

$$4NH_3 + 2NO + 2NO_2 \rightarrow 4N_2 + 6H_2O \quad (2)$$

$$4NH_3 + 3NO_2 \rightarrow 3.5N_2 + 6H_2O \quad (3)$$

$$4NH_3 + 6NO \rightarrow 5N_2 + 6H_2O \quad (4)$$

Among catalysts studied for NH_3-SCR, V_2O_5−WO_3/TiO_2, usually used for stationary NO_x reduction process,[42] is limited for applications in a mobile source. In fact, diesel engines operate under dynamic windows of temperature and flow. Hence, the required SCR catalyst needs a high efficiency at a high space velocity and also needs to be resistant to high temperatures induced by the diesel particulate filter (DPF) regeneration. Extensive efforts have been made to develop vanadium-free catalysts for the NH_3-SCR process. Supported transition metal, ceria-based oxides, or zeolites, such as $Fe_2O_3/WO_3/ZrO_2$,[43] MnOx−CeO_2,[44] CeO_2-zeolite,[45] Fe-ZSM-5[46,47] and Fe−Ce-ZSM-5,[48] have been proposed.

Recently, new catalytic systems, having high efficiency at low temperature and that are thermally stable up to 800 °C and have a limited impact of the NO_2/NO_x ratio on their activity, have been developed. Acidic zirconia mixed oxides are described as attractive alternatives for the NH_3-SCR application.[49] For instance, 50% NO conversion was attained at 250 °C for the standard SCR process. By applying the "fast" SCR conditions (NO_2/NO_x = 50%), 97% of NO_x was reduced to N_2 at only 200 °C.[50] The promotion of acidic zirconia by ceria also increases the NO_x conversion, the selectivity to N_2, and the catalyst durability. In fact, WO_3/CeO_2−ZrO_2 has been demonstrated to be efficient for the SCR of NO_x with NH_3 in diesel exhaust.[51] Studying the WO_3 loading on a CeO_2−ZrO_2 mixed oxide, a nearly complete NO_x conversion in a temperature range of 200−500 °C can be achieved with 10 wt % WO_3. Tungsten addition is found to enhance the activity of NO_x removal through the increase in acidic properties and NH_3 adsorption properties.[52] However, the effect of the support properties, that is, CeO_2/ZrO_2 (Ce−Zr) composition over a tungsten-supported catalyst, is not described in the literature, as far as we know.

The aim of this work is to study the ability of a WO_3/Ce−Zr SCR material to be added downstream to a model NSR catalyst (Pt/Ba−Al_2O_3) to maximize the N_2 yield of the process. The effect of the ceria−zirconia mixed oxide composition was studied at a constant WO_3 loading (9.1 wt % of WO_3). Acidic and basic properties of the SCR catalysts were measured, as well as their structural, textural, and redox properties. In fact, it is well-known that redox properties and acidity are necessary for the SCR reaction. The redox properties are suggested to control the reactivity at low temperature, whereas the acidic properties are expected to play a role in the SCR reaction at high temperature.[53] The solid properties for the selective catalytic reduction of NO_x with ammonia and the selective catalytic oxidation of ammonia (NH_3-SCO) were evaluated. Finally, the association between NSR and SCR phases is discussed, with a special attention to the use of the in situ-produced ammonia.

2. EXPERIMENTAL PART

2.1. Catalysts Preparation. Pure CeO_2 and ZrO_2 oxides and four $Ce_xZr_{1-x}O_2$ solid solutions, all provided by Rhodia, were used in this work as supports for the SCR catalysts. Solid solutions are noted Ce−Zr (wt % CeO_2−wt % ZrO_2), with a CeO_2 wt % of 70, 58, 40, and 20. All were first calcined 4 h under air at 600 °C before use. On these supports, 9.1 wt % of WO_3 was added by impregnation of the corresponding amount of ammonium metatungstate. This addition was carried out at 60 °C under continuous agitation. The preparation was then dried at 80 °C and placed in an oven overnight. Finally, the solid was calcined under wet synthetic air (10% H_2O) for 4 h at 700 °C. The obtained catalysts are noted WO_3/Ce−Zr.

A 1% Pt−10% BaO/Al_2O_3 catalyst was used as the NSR model catalyst. It was prepared by precipitation of the barium salt ($Ba(NO_3)_2$) on alumina powder, provided by Axens. First, the alumina was added to ultrapure water, and the temperature was raised to 60 °C. After the pH was increased to 10 by adding an ammonia solution, the dry barium salt was added. After drying at 120 °C, the support was calcined at 700 °C for 4 h under air. Platinum (1 wt %) was then impregnated using a Pt-$(NH_3)_2(NO_2)_2$ aqueous solution. After drying, the catalyst was pretreated at 700 °C for 4 h under N_2 and, finally, stabilized at 700 °C for 4 h under a mixture containing 10% O_2 and 10% H_2O in N_2. As previously reported,[54] the intermediate nitrogen treatment allows better platinum and barium dispersions. The obtained catalyst is noted Pt−Ba/Al. Its BET surface area is 161 $m^2\ g^{-1}$, with a mean pore size of 12 nm. The platinum dispersion, deduced from hydrogen chemisorptions, is 16%. The physicochemical characterizations of this sample are not fully detailed in this study, but it presents the usual characteristics as already reported for this kind of catalyst.[55,56]

Before being tested, solids were sieved between 100 and 250 μm.

2.2. Physical and Textural Properties. Nitrogen adsorption−desorption isotherms were recorded at −196 °C using a Tristar 3000 Micromeritics apparatus. Prior to the measurement, the samples were pretreated at 250 °C under vacuum for 8 h. The surface area was calculated using the BET model, the pore volume was evaluated at P/P_0 = 0.97, and the pore diameter was measured by using the BJH model applied to the desorption branch of the isotherms.

Catalysts were characterized by powder X-ray diffraction using a Bruker D5005 diffractometer equipped with a monochromatized Cu Kα radiation (λ = 1.5418 Å) operated at 40 kV and 30 mA. The diffraction patterns were recorded in the 2θ value range 15−75° with a step of 0.04° s^{-1} and a dwell time of 6 s. Crystalline phases were identified by comparison with ICDD database files.

2.3. Chemical Surface Properties. *2.3.1. Basic Properties.* According to the application of this work, basic properties were analyzed by NO_x storage capacity (NSC) measurements. Before analysis, the catalyst (60 mg) was pretreated in situ for 30 min at 550 °C, under a 10% O_2, 10% H_2O, 10% CO_2, and N_2 gas mixture

dx.doi.org/10.1021/cs3008329 | ACS Catal. 2013, 3, 1120−1132

Table 1. Catalytic Test Conditions[a]

catalytic tests	gas	NH_3, ppm	NO, ppm	H_2, %	O_2, %	CO_2, %	H_2O, %	N_2
NSR	rich			3		10	10	balance
	lean		500		10	10	10	
NH_3-SCR		500	500		10	10	10	balance
NH_3-SCO		500			10	10	10	balance

[a]Rich and lean gas compositions used for the NO_x conversion test in alternate cycles (60 s lean/3 s rich); NH_3-SCR and NH_3-SCO gas mixture. Lean mixture was used for the NO_x storage measurements. Total flow rate: 12 L h^{-1}.

(total flow rate: 12 L h^{-1}) and cooled to the storage temperature under the same mixture. The sample was then submitted to a lean mixture containing 500 ppm NO, 10% O_2, 10% H_2O, 10% CO_2, and N_2 (Table 1) at 200, 300, and 400 °C. The gas flow was introduced using mass-flow controllers, except for H_2O, which was introduced using a saturator. All gases, except diatomic gases, were followed by a MKS 2030 Multigas infrared analyzer. The NO_x storage capacity was estimated by the integration of the recorded profile for the first 60 s, which corresponds to the lean periods of the NSR test in cycling conditions (section 2.5.3). The contribution of the reactor volume is subtracted. For easier comparisons with the NSR tests, results are expressed as the NO_x storage rate (%) for 60s (100% corresponding to 99.2 μmol of NO_x/g, which can be stored by the catalyst).

2.3.2. Acidic Properties. NH_3 Storage. Acidic properties were carried out by ammonia storage measurements. The ammonia adsorption capacities were measured at three different temperatures: 200, 300, and 400 °C. Before analysis, the material (60 mg) was pretreated in situ under a feed gas similar to that of the NO_x storage experiments. A flow containing 500 ppm NH_3, 10% H_2O, 10% CO_2, and N_2 (total flow rate: 12 L h^{-1}) was injected until ammonia saturation of the material (300 s for all materials). Gas concentrations were determined by a Multigas infrared analyzer. The stored quantity of ammonia was calculated taking into account the reactor volume.

Pyridine Adsorption Followed by Infrared Spectroscopy. The surface acidity of the WO_3/Ce−Zr materials was evaluated by IR spectroscopy of the adsorbed pyridine. IR spectra were collected using a Nexus Nicolet spectrometer equipped with a DTGS detector (deuterium triglyceride sulfur) and KBr beam splitter. IR spectra were recorded using a resolution of 4 cm^{-1} and 64 scans. The spectra were normalized to a disc of 10 mg/cm^2. After activation at 450 °C, pyridine was adsorbed (200 Pa at equilibrium) at room temperature. Desorption was performed up to 450 °C in steps of 50 °C.

2.4. Redox Properties. *Temperature Programmed Reduction with Hydrogen (H_2-TPR).* Temperature programmed reduction (TPR) experiments were performed on a Micromeritics Autochem 2920 apparatus equipped with a thermal conductivity detector (TCD). A sample of ∼100 mg was placed in a U-shaped quartz reactor. Prior to the TPR measurements, the sample was calcined at 300 °C for 30 min under 10 vol % O_2 in Ar flow (temperature increase rate = 10 °C min^{-1}). The sample was cooled to room temperature and purged under Ar flow for 45 min. The reduction was carried out under 1 vol % H_2 in Ar flow up to 900 °C (temperature increase rate = 5 °C min^{-1}). Because the TCD signal is sensitive to water, a H_2O trap was added downstream of the reactor, allowing the quantification of the H_2 consumed during the TPR experiment.

Oxygen Storage Capacity (OSC). The OSC was measured at 400 °C under atmospheric pressure. The sample (5 mg) was continuously purged with helium (30 mL min^{-1}). Alternate pulses (0.265 mL) of pure O_2 and pure CO were injected every 2 min.[57] The oxygen storage capacity (OSC) was calculated from the CO_2 formation during alternate pulses of CO and O_2.

NO Oxidation Properties. The oxidation activity of the catalysts was estimated from the NSC measurements. At saturation (usually ∼900s), the NO_2/NO_x ratio (%) is constant and can be used to assess the NO-to-NO_2 oxidation activity of the catalysts in the limit of the thermodynamic equilibrium.

2.5. Catalytic Tests. *2.5.1. NH_3-SCR and NH_3-SCO Catalytic Tests.* The selective catalytic reduction (SCR) activity measurement was carried out in a quartz tubular microreactor under a flow simulating the realistic diesel engine exhaust conditions depicted in Table 1. A 60 mg portion of material was used in each run, and the total flow rate was fixed at 12 L h^{-1} (constant for all catalytic tests), corresponding to a GHSV of about 160 000 h^{-1} (GHSV, calculated as the volume of feed gas/volume of catalyst).

The compositions of the feed gas and effluent stream were monitored continuously using an online MKS Multigas infrared analyzer for gas analysis. The N_2 selectivity was calculated assuming no other N compounds than NO, NO_2, N_2O, and NH_3 are formed. The catalytic activity for NH_3-SCR of NO is expressed by the equation

$$X_{NO} = ([NO]_{inlet} - [NO]_{outlet})/[NO]_{inlet} \times 100\% \quad (5)$$

The SCO experiments were carried out using a protocol similar to that previously depicted for the SCR test, except that NO was replaced by the same flow of nitrogen (Table 1).

2.5.2. Kinetic Parameters. Steady-state kinetic experiments were carried out in a fixed-bed reactor. Kinetic orders were determined using 60 mg of catalyst. The typical reactant gas composition was as follows: 200−1600 ppm NO, 200−1600 ppm NH_3, 10% O_2, 10% H_2O, 10% CO_2, and N_2. Practically, the NO or NH_3 concentration was fixed at 1600 ppm, whereas the concentration of the other reactant was increased from 200 to 1000 ppm. The reaction temperature was controlled by a programmable temperature controller, and NH_3 or NO conversions were fixed at 10% in most cases.

Apparent activation energies E_a were determined from the catalytic tests of NH_3-SCR and NH_3-SCO. The Arrhenius law ($\ln(NH_3\ conv.) = f(1/T)$) was applied to calculate the apparent E_a of NH_3-SCR or NH_3-SCO for low ammonia conversions (<20%).

2.5.3. NO_x Storage Reduction Tests (Cycled Conditions). NO_x storage reduction experiments were performed using NSR catalyst alone (NSR tests, 60 mg of Pt−Ba/Al + 120 mg of inert SiC), or in association with a SCR material downstream (NSR + SCR combined system, 60 mg of Pt−Ba/Al + 120 mg of SCR catalyst). Before measurement, the catalytic bed was treated in situ at 450 °C under 3% H_2, 10% H_2O, 10% CO_2, and N_2 for 15 min. The sample was then cooled to reaction temperatures (200, 300, and 400 °C) under the same mixture. NO_x conversions were measured in cycling conditions by alternately switching between lean and rich gas mixtures using electrovalves. The lean and rich periods were 60 s and 3 s, respectively. The gas composition is

dx.doi.org/10.1021/cs3008329 | ACS Catal. 2013, 3, 1120−1132

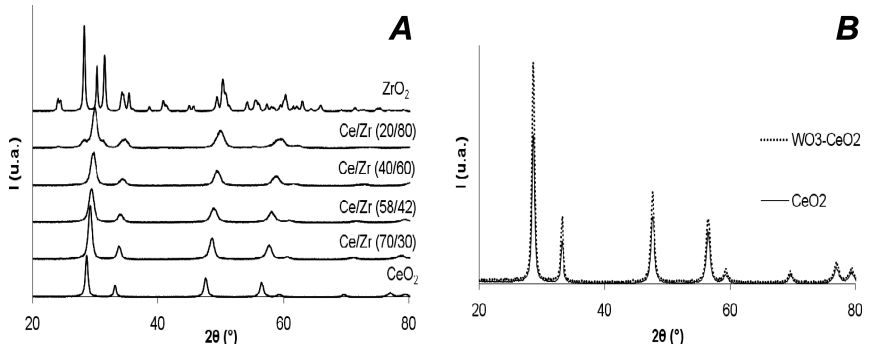

Figure 1. XRD patterns of (A) ceria−zirconia supports and (B) the effect of WO_3 impregnation on CeO_2.

Table 2. Physical Properties of WO_3-Supported Catalysts Calcined under Hydrothermal Treatment at 700°C

Ce−Zr ratio	XRD analysis	crystal phase	S_{BET} (m^2 g^{-1}) catalyst (support)	d_{BJH} (nm)
CeO_2	CeO_2	cubic	23 (42)	13.9
(70−30)	$Ce_{0.6}Zr_{0.4}O_2$	cubic	27 (62)	16.3
(58−42)	$Ce_{0.5}Zr_{0.5}O_2$	tetrahedral	53 (61)	10.5
(40−60)	$Ce_{0.32}Zr_{0.68}O_2$	tetrahedral	55 (64)	17.1
(20−80)	$Ce_{0.15}Zr_{0.85}O_{2+Ce0.02Zr0.98O2}$	tetrahedral (70%) + monoclinic (30%)	74 (60)	10.3
ZrO_2	ZrO_2	monoclinic	31 (19)	22.0

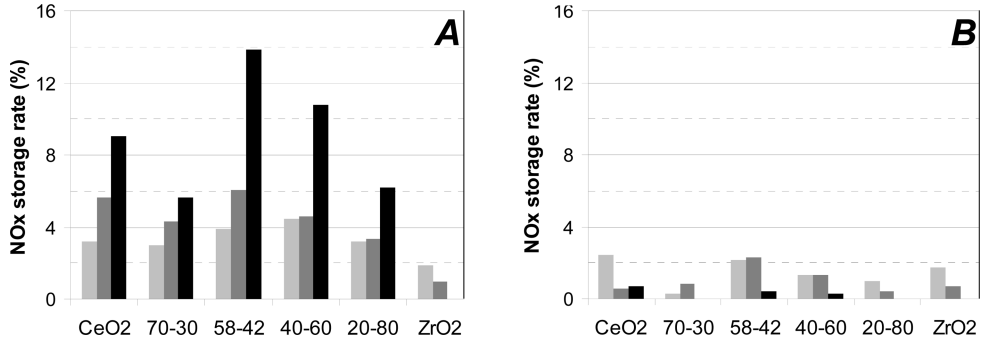

Figure 2. NO_x storage capacity rate (%) calculated for 60 s of (A) ceria−zirconia supports and (B) WO_3 supported catalysts at 200 °C (light gray), 300 °C (medium gray) and 400 °C (black).

described in Table 1. Note that only the stored NO_x during the lean periods can be reduced using this procedure, since there is no reductant in the lean mixture and no NO_x in the rich one. Most gases (NO, NO_2, N_2O, NH_3, CO, CO_2, etc.) were analyzed using a Multigas FTIR detector (MKS 2030), except H_2, which was analyzed by mass spectrometry.

3. RESULTS AND DISCUSSION

3.1. Physical and Textural Properties of WO_3/Ce−Zr Catalysts. Physical and textural properties of ceria−zirconia supports were first characterized using both N_2 adsorption isotherms and XRD analysis. XRD patterns are presented in Figure 1. Before WO_3 impregnation (Figure 1A), XRD phase analysis of CeO_2−ZrO_2 mixed oxides showed only the presence of single phase solid solutions, which differ from the zirconia loading. The pure CeO_2 sample calcined at 600 °C was composed of cubic CeO_2 with fluorite structure at 2θ = 28.8, 47.7, and 56.5°.[58] The addition of zirconia to ceria leads to a shift of XRD peaks to higher values and, for the highest loading, to the appearance of characteristic peaks corresponding to monoclinic zirconia at 2θ = 30.3, 50.5, and 44.8°. For instance, the Ce−Zr (58−42) support shows a broad band that was observed at 2θ = 29.1° between pure c-CeO_2 (28.4°, JCPDS 34-0394) and pure t-ZrO_2 (30.2°, JCPDS 79-1766). It is attributed to $Ce_{0.5}Zr_{0.5}O_2$ solid solution (~3 nm) due to the replacement of Ce^{4+} ions (0.97 Å) by the smaller Zr^{4+} ions (0.84 Å), in agreement with XRD diffraction database (JCPDS 38-1436) and results obtained from the literature.[59,60]

The XRD analyses are otherwise reported in Table 2. After WO_3 impregnation, no modification of XRD patterns is observed, as reported in Figure 1B for the CeO_2-supported sample. In addition, no WO_3 XRD peaks are detected, suggesting a good dispersion of the tungsten trioxide phase, as expected. Indeed, Li et al.[61] reported that tungsten oxide can be highly dispersed on $Ce_{0.5}Zr_{0.5}O_2$ solid solution, with a dispersion capacity of ~8 μmol/m^2. In this work, 9.1 wt % of WO_3 supported on various CeO_2−ZrO_2-based oxides were prepared with specific surface areas of host supports ranked between 19 m^2 g^{-1} (pure ZrO_2) and 60−64 m^2 g^{-1} (Ce−Zr supports). Impregnation of 9.1 wt % WO_3 (390 μmol/g) may form a monolayer WO_3 dispersion over the Ce−Zr supports (surface concentration of ~6 μmol/m^2). The supported tungsten oxide species are rather preferentially interacting with ceria component on the surface of Ce−Zr mixed oxides.[61] In fact, the results of N_2 adsorption isotherms of supports and WO_3-supported catalysts (Table 2) confirm different interactions between WO_3 and ceria or zirconia.

dx.doi.org/10.1021/cs3008329 | ACS Catal. 2013, 3, 1120−1132

Table 3. Ammonia Storage (μmol/g) until Saturation (usual duration, 300s) on Ceria−Zirconia and WO_3/Ce−Zr Samples (60 mg) under 500 ppm NH_3, 10% H_2O, 10% CO_2 + N_2 (12 L h^{-1})

	ceria−zirconia			WO_3/Ce−Zr		
materials	200 °C	300 °C	400 °C	200 °C	300 °C	400 °C
CeO_2	0	0	0	43	15	5
Ce−Zr (70−30)	8	0	0	27	15	3
Ce−Zr (58−42)	11	2	0	68	28	12
Ce−Zr (40−60)	10	2	0	78	29	20
Ce−Zr (20−80)	15	2	0	82	40	18
ZrO_2	12	5	3	71	35	13

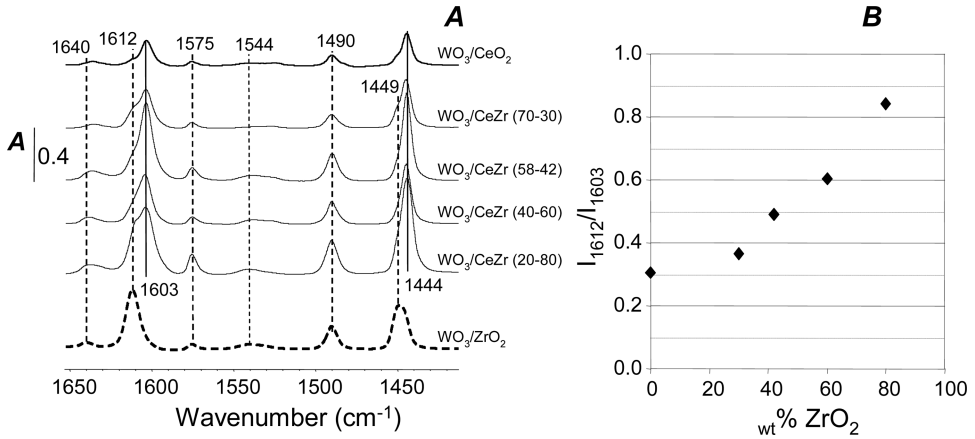

Figure 3. (A) Infrared spectra of pyridine adsorbed on WO_3/CeZr-based catalysts at room temperature (200 Pa), followed by evacuation at 150 °C. (B) Relationship between the $I_{(1612)}/I_{(1603)}$ ratio versus the ZrO_2 weight content of WO_3/CeZr-based catalysts.

For the ceria-rich compositions, until Ce−Zr (40−60), addition of WO_3 leads to a decrease in the specific surface area. In contrast, the specific surface areas of Ce−Zr (20−80)- and pure ZrO_2-supported catalysts increase after WO_3 addition. Finally, the specific surface areas of the Ce−Zr-supported catalysts increase with the zirconia loading.

3.2. Chemical Surface Properties of WO_3/Ce−Zr Catalysts. Basic properties of SCR materials (WO_3/Ce−Zr) were characterized by NO_x storage measurements, in line with the furthermore association in the NSR + SCR process. The characterization of the acidic properties was studied evaluating both the NH_3 storage capacity and the pyridine adsorption monitored by IR spectroscopy.

3.2.1. NO_x Storage. The NO_x storage capacities were measured at 200, 300, and 400 °C in a lean mixture containing H_2O and CO_2. The fractions of stored NO_x for 60 s are reported in Figure 2.

It appears that for the ceria−zirconia supports, the NO_x storage rate constantly grows with temperature, especially when the temperature reaches 400 °C. In fact, the NO_x adsorption depends mainly on the first step of the process, that is, the NO oxidation into NO_2. To assess the oxidation activity of catalysts, the NO/NO_2 ratio is calculated at saturation. This point is developed in the following sections, but it can be noticed that the higher the temperature, the higher the NO/NO_2 ratio. Finally, the higher NO_x storage capacity is obtained with the Ce−Zr (58−42) sample at 400 °C, but it reaches only 14% (Figure 2A). For comparison, a model NSR catalyst (1% Pt/BaO−Al_2O_3[62]) reaches a NO_x storage of ∼80−90% under similar conditions (section 3.5.1, Figure 8). As expected, pure ZrO_2 exhibits very low NO_x storage behavior, with no storage at 400 °C.

When WO_3 is added to Ce−Zr supports, Figure 2B shows that the amount of stored NO_x dramatically drops and is not meaningful. This result confirms the previous XRD analyses that indicate a good WO_3 dispersion. The basic NO_x storage sites are covered by the acidic WO_3 oxide.

3.2.2. NH_3 storage. The acidic properties were evaluated by measuring the ammonia storage capacity at 200, 300, and 400 °C under dynamic conditions. The results are reported in Table 3. As expected, the ammonia storage capacity decreased with increasing temperature, showing that the strength of the acidic sites of the studied supports is rather weak. Without tungsten, only pure zirconia is able to store ammonia at 400 °C. Contrasting with the NO_x storage capacity, the NH_3 storage rate is strongly improved when tungsten trioxide is impregnated on ceria−zirconia mixed supports (Table 3). Even if tungsten significantly increases the acidity of ceria, WO_3/ZrO_2 again stores more ammonia than WO_3/CeO_2. For the WO_3/Ce−Zr materials, the increase in the zirconium content enhances the acidity (number and strength of acidic sites). Among the tested supports, WO_3/Ce−Zr (20−80) presents the higher amount of acid sites.

3.2.3. Pyridine Adsorption Followed by IR. Pyridine is one of the most largely used basic probe molecule to characterize the surface acidity of solids.[63−65] In the present case, infrared spectroscopy of adsorbed pyridine was used to determine the influence of the ceria−zirconia ratio on the nature of the acid sites of the WO_3 supported catalysts. The IR spectra of samples obtained after pyridine evacuated at 150 °C are depicted in Figure 3 for the frequency range of the ring ν_{CCN} vibration (1650−1400 cm^{-1}). Characteristic frequencies of pyridine coordinated to Lewis acid sites (LAS) were observed at 1444−1449 cm^{-1} (ν_{19b}), 1490 cm^{-1} (ν_{19a}), 1578 cm^{-1} (ν_{8b}), and at

dx.doi.org/10.1021/cs3008329 | ACS Catal. 2013, 3, 1120−1132

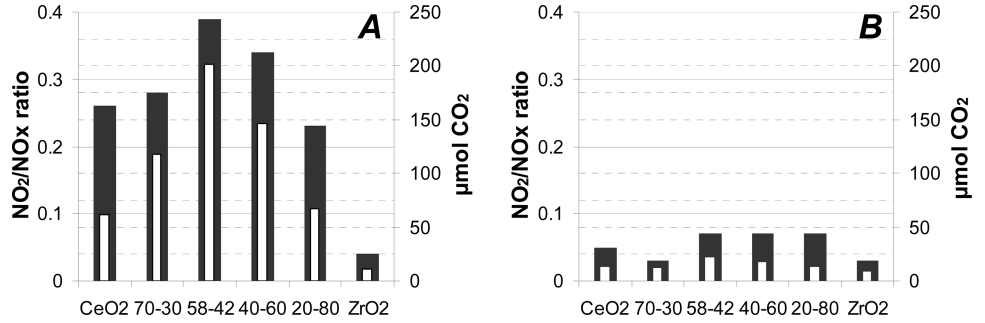

Figure 4. OSC (□) and NO to NO_2 oxidation activity (■) calculated at 400 °C from (A) ceria−zirconia supports and (B) WO_3 supported catalysts.

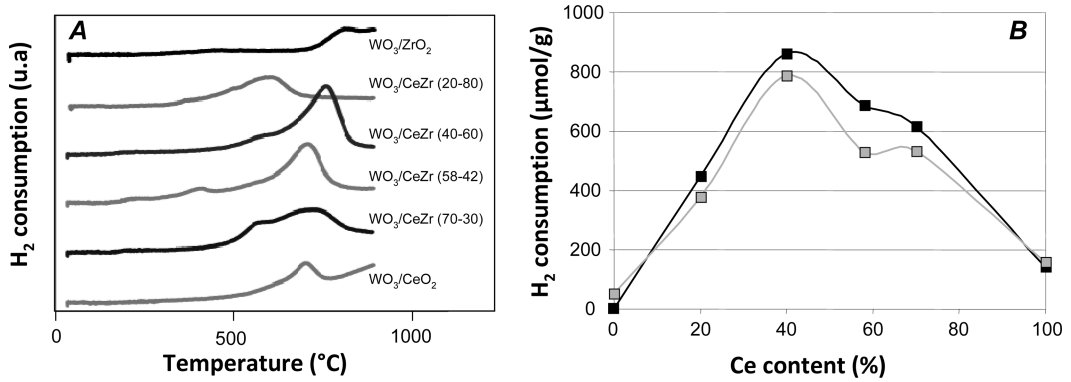

Figure 5. (A) TPR profiles of WO_3/Ce−Zr catalysts. (B) H_2 consumption (μmol g^{-1}) corresponding to the "easily" reducible Ce^{IV} of the Ce−Zr supports (black) and WO_3-supported catalysts (gray) deduced from the TPR measurements.

1603−1612 cm^{-1} (ν_{8a}). Formation of pyridinium surface species is characterized by ν_{8a} absorption at 1640 cm^{-1} in association with the ν_{19b} absorption mode at 1544 cm^{-1}. These results are in accordance with the study of Larsen et al.,[66] which reports the IR spectra of pyridine adsorbed on tungstated zirconia.

The position and the multiplicity of the ν_{8a} ring vibration of chemisorbed pyridine on Lewis acid sites (1579 cm^{-1} in liquid phase) is related to their nature, their number, and their strength.[67] On pure ceria, Tamura et al.[68] observed ν_{8a} absorption at 1597 cm^{-1} after pyridine evacuation at 150 °C, compared with ν_{8a} absorption at 1604−1605 cm^{-1} on ZrO_2.[69]

The occurrence of the ν_{8a} vibration mode at two different frequencies (1603 and 1612 cm^{-1}) on tungstated ceria−zirconia likely indicates the presence of heterogeneous Lewis acid sites having different strengths.[70−73] The ratio between the intensity of the ν8a doublet (I_{1612}/I_{1603}) allows us to follow the enhancement of the relative amount of LAS versus the ZrO_2 weight content on tungstated ceria−zirconia-based oxides. Figure 3B reveals that the higher the amount of zirconia loading, the higher the amount of strong LAS. In contrast, on pure WO_3/ZrO_2, only one kind of LAS is observed (ν_{8a} at 1612 cm^{-1}). This result is in accordance with the literature that denotes ν_{8a} absorption at 1610 cm^{-1} over a tungstated zirconia sample.[74,75] Moreover, the addition of WO_3 to CeO_2−ZrO_2 host supports also leads to the formation of Brønsted acid sites, not relevant on pure oxides.[76] The Brønsted acid sites are then linked to the addition of WO_3.

To conclude, in addition to ammonia storage experiments (section 3.2.2), the acidic characterization by FTIR reveals that both Lewis and Brønsted acid sites are present over all the studied catalysts. Brønsted acid sites are not dominant, and LAS with higher strength are enhanced with the Zr content of the host support.

3.3. Redox Properties of WO_3/Ce−Zr Catalysts. First, redox properties were evaluated in terms of OSC- and NO-to-NO_2 oxidation activity (NO/NO_2 ratio calculated at saturation during the NO_x storage tests), both measured at 400 °C. Results are presented in Figure 4 for ceria−zirconia mixed samples and WO_3-supported catalysts.

It appears that both OSC and the NO/NO_2 ratio show parallel evolution for the ceria−zirconia-based supports (Figure 4A). The optimal redox properties are obtained with formulations close to the 50/50 ratio: namely, Ce−Zr (58−42 and 40−60). For instance, a NO/NO_2 ratio higher than 30% is obtained with the Ce−Zr (58−42) sample, which is quite close to a usual NSR catalyst.[54] These NO oxidation properties are in accordance with previous NO_x storage measurements depicted in Figure 2A. In fact, Ce−Zr (58−42 and 40−60) provides both the higher NO-to-NO_2 oxidation properties and the higher NO_x storage capacity at 400 °C.

Over tungstated materials, Figure 4B reveals that both OSC and the NO/NO_2 ratio are significantly lowered compared with the host supports. Note that the low NO_2/NO_x ratio at 0.03 for WO_3/Ce−Zr (70−30) and WO_3/ZrO_2 corresponds to the observed ratio without a catalyst. These two materials exhibit the lower oxygen mobility/oxygen activation behaviors, with no NO oxidation capacity.

Second, redox properties were evaluated in terms of reducibility by hydrogen using TPR experiments. The H_2 reduction of ceria−zirconia-based oxides is well-known (curves not shown), and without a noble metal, a main reduction peak is observed in the 550−620 °C temperature range, depending on the material composition. It corresponds to the easily reducible Ce^{IV} reduction in Ce^{III}: the higher the zirconium content, the lower the temperature peak. The corresponding H_2 consumptions (μmol g^{-1}) are plotted in Figure 5. Ce−Zr supports show a

dx.doi.org/10.1021/cs3008329 | ACS Catal. 2013, 3, 1120−1132

Table 4. NH_3, NO_2, and NO_x Concentrations at 400 and 500°C during the NH_3-SCR Test Performed on Ceria−Zirconia Supports

	400 °C				500 °C			
materials	NH_3 consumed (ppm)	NO_2 detected (ppm)	NO_x formed (ppm)	N_2[a] formed (ppm)	NH_3 consumed (ppm)	NO_2 detected (ppm)	NO_x formed (ppm)	N_2[a] formed (ppm)
CeO_2	23	124	3	9	142	117	98	19
Ce−Zr (70−30)	76	120	14	29	254	118	179	33
Ce−Zr (58−42)	94	150	54	12	287	173	237	16
Ce−Zr (40−60)	108	126	68	13	264	161	214	15
Ce−Zr (20−80)	191	111	123	27	355	131	285	27
ZrO_2	22	14	−10	14	186	22	90	43

[a]The N_2 formation is calculated taking into account the variation of NH_3, NO_x, and N_2O concentration. Note that the N_2O emission (note reported) is ranked between 1 and 10 ppm, depending on the temperature and the support formulation.

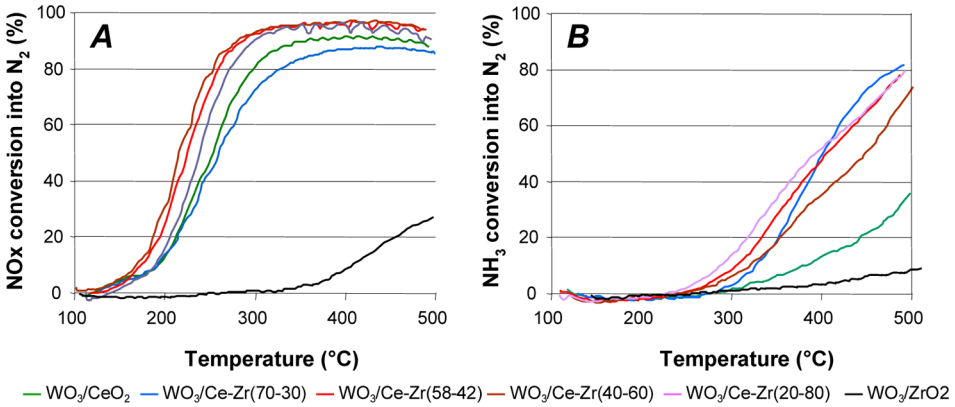

Figure 6. (A) NO_x conversion into N_2 under 500 ppm NH_3, 500 ppm NO, 10% O_2, 10% H_2O, 10% CO_2 + N_2 and (B) NH_3 conversion into N_2 under 500 ppm NH_3, 10% O_2, 10% H_2O, 10% CO_2 + N_2 on WO_3/Ce−Zr from 100 to 500 °C.

H_2 consumption only when Ce is present. Ceria−zirconia 70−30, 58−42, and 40−60 present the highest H_2 consumptions, as already reported in ref 77. Ce−Zr (40−60) is the more reducible support, with 860 μmol/g of H_2 consumed. After WO_3 addition (Figure 5A), a shift of ∼80−100 °C to higher reduction temperatures is observed. Moreover, H_2 consumption decreases by nearly 10% after addition of WO_3, as depicted in Figure 5. Nevertheless, Ce^{IV} reduction of supports is only slightly affected. The WO_3/ZrO_2 TPR profile shows a H_2 consumption only at elevated temperatures (more than 800 °C), which probably indicates a WO_3 reduction.[78,79]

Note that the most reducible ceria−zirconia supports (70−30, 58−42, and 40−60) likewise present the higher oxygen storage capacity, too; however, the Ce−Zr TPR profiles show no or really weak H_2 consumption before 400 °C (Figure 5A), so no relationship can be assumed between OSC measurement (CO as reductant) and reducibility by H_2 at this temperature.

3.4. Catalytic Activities. *3.4.1. NO_x SCR with NH_3.* First, the Ce−Zr supports were evaluated for the NO_x SCR with NH_3 from 100 to 500 °C (light-off type tests). On pure ceria and zirconia, no activity is observed below 300 °C. Gas concentrations (NH_3, NO_2, NO_x, and N_2) obtained at 400 and 500 °C are then depicted in Table 4. Except for pure ZrO_2 at 400 °C, it is reported that supplementary NO_x are detected, indicating that the main reaction is the ammonia oxidation into NO_2, but N_2 formation also occurs. On pure zirconia, the SCR reaction is the major reaction at 400 °C, with 2% of NO_x conversion. Note that on the whole materials, the NH_3 conversion ranks between 2 and 6% at 400 °C and does not exceed 9% at 500 °C. However, it is noticeable that the higher the zirconium content, the higher the quantity of converted ammonia. At the same time, NO_x detection increases, indicating that ammonia is oxidized mainly into NO_x.

The amounts of formed NO_2 follow the NO_2/NO_x ratios obtained in Figure 4A, with a maximum reached for Ce−Zr (58−42). Finally, during the SCR experiments, very little N_2O is detected, at ∼4−7 ppm, whatever the samples.

Second, WO_3/Ce−Zr materials were tested in NH_3-SCR (Figure 6A). Except for WO_3/ZrO_2, which oxidized a part of the ammonia by O_2 into nitrogen (at a maximum nearly 20 ppm NH_3 at 500 °C, with an SCO-to-SCR ratio close to 15%), only the reaction of NO_x reduction into nitrogen by ammonia is observed. Indeed, NO_x and NH_3 concentrations decrease together throughout the temperature. In addition, a low N_2O concentration was detected (1−5 ppm), in contrast with copper zeolite, for instance.[80] WO_3/ZrO_2 is significantly less active than the other catalysts and provides a maximum NO_x conversion into N_2 of ∼25% at 500 °C. The five other materials exhibit maximum NO_x conversion into N_2 higher than 80%. WO_3/Ce−Zr catalysts are then very active to reduce nitric oxides with NH_3, with 50% of NO_x conversion obtained at the 210−255 °C temperature range. To compare, iron zeolite, largely studied in the literature, converts 50% of NO_x from 345 to 390 °C[81,82] under a similar gas feed composition.

WO_3/CeO_2 and WO_3/Ce−Zr (70−30), which are the less active, are structured in a cubic system, WO_3/Ce−Zr (20−80) which show intermediate results containing a tetrahedral (70%) and monoclinic (30%) system, whereas the most active catalysts (WO_3/Ce−Zr (58−42 and 40−60)) are structured in a tetrahedral system only, so it seems thatthe tetrahedral structure of ceria−zirconia obtained with a weight ratio close to 50/50 promotes the SCR-NH_3 activity for WO_3/Ce−Zr materials.

According to refs 83 and 84, the beneficial impact of W on the Ce^{3+}/Ce^{4+} ratio distribution could be a possible reason for the SCR enhancement. However, an increase in the oxygen vacancies

dx.doi.org/10.1021/cs3008329 | ACS Catal. 2013, 3, 1120−1132

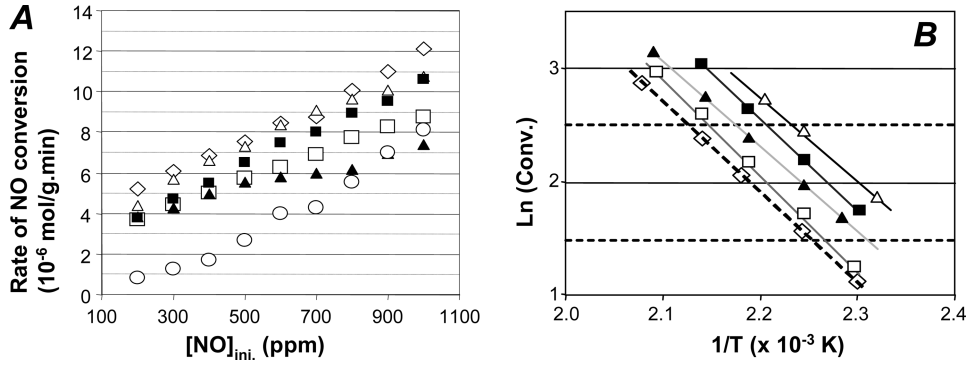

Figure 7. Determination of kinetic parameters over WO_3/Ce−Zr catalysts with 60 mg of catalyst, 1500 ppm NH_3, 200−1000 ppm NO, 10% O_2, 10% H_2O, and 10% CO_2. (A) Dependence of the NO conversion rate on the NO concentration and (B) the Arrhenius plot of the logarithm of the conversion (160−205 °C). (◊) CeO_2, (□) 20−80, (△) 40−60, (■) 58−42, (▲) 70−30, and (○) ZrO_2.

ratio is usually associated with an increase in the redox properties of ceria. In contrast, OSC and TPR measurements show a decrease in the redox behavior on WO_3/Ce−Zr catalysts compared with ceria−zirconia supports.

These NH_3-SCR tests also put in evidence possible ammonia oxidation by O_2. With the aim of a NSR + SCR combined system, NO_x and ammonia should not be simultaneously introduced. NO_x are supposed to react with adsorbed ammonia over the SCR catalyst during the lean phases in large oxygen excess. Then O_2−NH_3 reactivity was also studied.

3.4.2. NH_3-SCO. The results of NH_3 oxidation by O_2 are presented in Figure 6B. During these experiments, N_2O was not detected. In addition, the ammonia oxidation is nearly fully selective to N_2, since NO_x (in fact, NO) were observed only for WO_3/ZrO_2 and WO_3/Ce−Zr (70−30) at a very low extent (no more than 20 ppm at 500 °C for both of them). These two materials have previously showed the smallest OSC and NO to NO_2 oxidation capacities (Figure 4B), so for these catalysts, it seems that the low mobility of activated oxygen leads to the possible NH_3 oxidation by O_2 into NO_x at elevated temperature (T > 350 °C). If all the materials start to oxidize ammonia at ∼250 °C, activities become different at higher temperatures. As under NH_3-SCR conditions, WO_3/ZrO_2 is the less active catalyst in ammonia oxidation by O_2, probably because of its lower surface area and its negligible reducibility (Figure 5). WO_3/CeO_2, which also possesses a weak reducibility, slightly oxidizes ammonia by O_2. The other four materials based on Ce−Zr mixed supports show rather close activities for ammonia oxidation, with almost 80% of maximum ammonia converted at 500 °C, nearly exclusively into N_2.

3.4.3. Kinetics Parameters. For determining the reaction order with respect to NO, the concentration of NH_3 was kept at 1600 ppm while the concentration of NO was varied from 200 to 1000 ppm. The reaction order was determined at fixed temperature for limited NO conversion at around 10−15% (corresponding to a temperature range of 180−200 °C, depending on the catalytic formulation).

Figure 7A shows the rate of NO conversion as a function of NO concentration, depending on the WO_3-supported catalysts. It appears that the rates of NO consumption were found to increase linearly with NO concentration at all temperatures; hence, the reaction rate of NO consumption as a function of reactant concentrations can be expressed simply as a power-law rate equation, since O_2, CO_2, and H_2O are largely in excess in the feed gas (∼10% for each compound):

$$r_{NO} = k_a[NH_3]^{\alpha}[NO]^{\beta} \quad (6)$$

$$\text{with } k_a = k[O_2]^x[CO_2]^y[H_2O]^z$$

where r_{NO} is the SCR rate; k_a is the apparent rate constant, defined as above; and α, β are the reaction orders for NO and NH_3, respectively. Results are reported in Table 5. According to the above data, the NO reaction order is close to 0.5 (ranging from 0.36 to 0.63) for ceria-containing supports, The value obtained with WO_3/ZrO_2 is nearly three times higher than on the other materials, corresponding to a limited NO_x coverage. In addition, WO_3/ZrO_2 material exhibits a poor NO_x storage capacity. These tendencies are consistent with the low NH_3-SCR activity of this catalyst described previously in Figure 6A.

Table 5. Kinetic Parameters, E_a (kJ/mol), and NH_3 and NO Kinetic Orders for WO_3/Ce−Zr Materials

	E_a (kJ/mol)		NH_3-SCR kinetic order	
materials	NH_3-SCR	NH_3-SCO	NO	NH_3
WO_3/CeO_2	40	58	0.45	−0.16
WO_3/Ce−Zr (70−30)	48	119	0.36	−0.20
WO_3/Ce−Zr (58−42)	68	100	0.63	−0.23
WO_3/Ce−Zr (40−60)	61	86	0.55	−0.25
WO_3/Ce−Zr (20−80)	74	94	0.54	−0.39
WO_3/ZrO_2	100	39	1.51	−0.11

Similar experiments were performed to determine the reaction order with respect to NH_3. Results are summarized in Table 5. An inhibition by NH_3 with negative reaction order ranging from −0.11 to −0.39 was demonstrated. By increasing the zirconium content in ceria, WO_3/Ce−Zr catalysts become more acidic (Table 3). Values of the NH_3 kinetic orders, which also become more negative with an increase in the zirconium content, are then in line with the acidic characterization.

From results obtained in NH_3-SCR and NH_3-SCO experiments, the respective apparent activation energies were determined using the Arrhenius law in the 0−20% conversion range. The activation energies of WO_3-supported catalysts for the NH_3-SCR reaction depend on the ceria−zirconia formulation, as shown in Figure 7B, but they remain quite close, as depicted in Table 5. For instance, increasing the zirconium content leads to an increase in the $E_{a_{SCR}}$ value, from 40 to 74 kJ/mol for WO_3/CeO_2 and WO_3/Ce−Zr (20−80) catalysts, respectively. In contrast, the $E_{a_{SCR}}$ of WO_3/ZrO_2 reaches 100

dx.doi.org/10.1021/cs3008329 | ACS Catal. 2013, 3, 1120−1132

kJ/mol (not shown in Figure 7B). This reveals that the activity of WO_3-supported catalysts is correlated to the amount of NO and NH_3 adsorbed on the catalyst surface, so increasing the zirconium content in these materials is damaging for the SCR-NH_3 reaction. Nevertheless, the frequency factors of the Arrhenius equation, supposed to indicate the number of active sites on the catalyst surface, also vary with respect to the zirconia content (Figure 7B).

Similarly, the apparent activation energies were determined for the NH_3-SCO reaction. The results are reported in Table 5 (curves not shown). For this reaction, there is no clear evolution of the apparent $E_{a_{SCO}}$. WO_3/ZrO_2 possesses the weakest apparent energy (39 kJ/mol), compared with 58 kJ/mol for WO_3/CeO_2. Zirconium incorporation into the mixed oxides led to a strong increase in the apparent $E_{a_{SCO}}$, up to 119 kJ/mol for WO_3/Ce−Zr (70−30). Then, the apparent $E_{a_{SCO}}$ slightly decreases with the increase in the zirconium content, until 94 kJ/mol for WO_3/Ce−Zr (20−80).

The comparison of NH_3-SCR and NH_3-SCO apparent activation energies (Table 5) indicate that only the catalyst supported over pure zirconia favors the ammonia oxidation by O_2. This result is in agreement with the NH_3-SCR catalytic test, which shows that WO_3/ZrO_2 is the only sample that oxidizes ammonia in nitrogen by oxygen.

To conclude, the kinetic orders, as well as apparent activation energies obtained in this work, are in agreement with the literature, which describes the NH_3-SCR mechanism as a reaction between adsorbed ammonia and NO from the gas phase (or weakly adsorbed).[43,85−87] The reaction order is positive for NO and negative for NH_3 and depends little on the zirconia loading. Ammonia-SCR is self-inhibited by NH_3, suggesting that NH_3 adsorption is the determining step of the process as for NH_3-SCR occurring over exchanged-based zeolites materials.[88]

3.5. NO_x Reduction Catalytic Tests. *3.5.1. NSR Behaviors of Pt−Ba/Al.* First, the NO_x storage rate, NSR efficiency, and ammonia selectivity of the Pt−Ba/Al model catalyst were studied using 60 mg of Pt−Ba/Al and 120 mg of inert SiC to replace the SCR catalyst. The results are presented in Figure 8.

Whatever the tested temperatures, the NO_x conversion is always lower than the NO_x storage rate for 60 s. The maximum

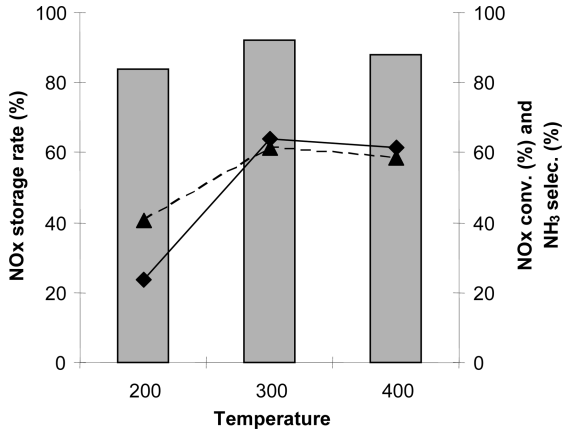

Figure 8. NO_x storage rate (%) calculated for the first 60 s (bars), NO_x conversion (−), and NH_3 selectivity (---) in cycled conditions for a model Pt−Ba/Al NSR catalyst at 200, 300, and 400 °C in cycled conditions.

NO_x conversion is obtained at 300 °C and reaches about 64% (solid line, Figure 8). In the same time, only 36−82% of the introduced hydrogen is converted. Thus, reductants remain (H_2, NH_3), whereas only a part of the stored NO_x reacts. The limiting step of the process is then the reduction step. In addition, the ammonia selectivity is rather high. It increases from around 40% at 200 °C to ~60% at 300 and 400 °C (dotted line, Figure 8). The amount of NH_3 emitted from this catalyst, which is expected to be used on the NSR catalyst, is reported in Table 6. Finally, note that N_2O was never observed during these tests in cycling condition.

3.5.2. NSR + SCR Combination System. NO_x reduction efficiency was studied in a dual NSR + SCR catalytic bed (60 mg of Pt−Ba/Al + 120 mg of SCR catalyst). In this part, only active materials in NH_3-SCR were considered: namely, all the materials WO_3/Ce−Zr except WO_3/ZrO_2. Lean (60s)/rich (3s) cycling experiments were performed at 200, 300, and 400 °C, as already presented in Figure 8 for the single Pt−Ba/Al model catalyst. Concentrations of the different nitrogenous gases (NO, NO_2, N_2O, NH_3) were taken into account after stabilization. Figure 9 presents the NO_x conversion (into ammonia or nitrogen) for the coupled NSR + SCR catalytic system. Results presented previously with the NSR catalyst alone are also added. An example of the nitrous compound profiles obtained withthe NSR catalyst alone and with the Pt−Ba/Al + WO_3/Ce−Zr (58−42) combined system is depicted in Figure 10. This example clearly shows that the addition downstream of an active NH_3-SCR material is a workable solution to enhance the NO_x conversion. As expected from SCR and SCO tests, N_2O was not detected in all the tests performed with NSR + SCR coupled system, as already mentioned with NSR catalyst alone.

NO_x conversion described in Figure 9 shows that the addition of WO_3/Ce−Zr materials promotes NO_x conversion into nitrogen, whatever the tested temperatures and the considered SCR catalyst. However, ammonia reactivity varies with the temperature and the nature of the SCR catalyst. First, the in situ-produced ammonia over the first catalytic bed is fully converted at 200 °C. In contrast, at 300 °C and, in addition, at 400 °C, some NH_3 is still released, which can be linked to a lack of acid storage sites over the SCR catalysts. The relationship between unconverted NH_3 at 400 °C (ppm) emitted from the NSR + SCR combination and acid sites concentration determining by NH_3 storage measurement at 400 °C (μmol/g) over WO_3/Ce−Zr-supported catalysts is presented in Figure 11.

There is a good correlation between the ammonia storage capacity and the amount of unconverted NH_3: the higher the amount of unconverted NH_3 at 400 °C in SCR materials, the lower the acidic sites concentration. This result is globally in accordance with the kinetic orders determined for NH_3 in the SCR reaction (Table 5): the higher the catalyst acidity, the more negative the kinetic order for NH_3.

In addition to the possible ammonia slip, adsorbed ammonia over WO_3/Ce−Zr catalysts reacts during the lean phases (in O_2 excess) following both the SCR and the SCO reactions. Table 6 reports, for the three tested temperature, the amount of NH_3 emitted from the model NSR sample and the ammonia used over the second catalytic bed, with regard to the NH_3-SCR and the NH_3-SCO reactions, and the unconverted NH_3. The ammonia consumed by the NH_3-SCR reaction was calculated considering that each additional converted NO_x is associated with one converted molecule of ammonia. Supplementary ammonia conversion is associated with the SCO reaction, considering a fully selective reaction into N_2, as demonstrated in section 3.4.2.

dx.doi.org/10.1021/cs3008329 | ACS Catal. 2013, 3, 1120−1132

Table 6. Ammonia Used Distribution on the Second Catalytic Bed (%)

			distribution of ammonia on second bed (%)		
materials	T (°C)	NH_3 emitted by NSR (ppm) (60 mg)	NH_3-SCR (120 mg)	NH_3-SCO (120 mg)	Unconverted NH_3 (120 mg)
WO_3/Ce−Zr (20−80)	200	48	108[a]	0	4
	300	174	68	23	9
	400	171	46	41	13
WO_3/Ce−Zr (40−60)	200	48	156[a]	0	2
	300	174	50	47	3
	400	171	32	57	11
WO_3/Ce−Zr (58−42)	200	48	156[a]	0	2
	300	174	43	35	23
	400	171	48	10	42
WO_3/Ce−Zr (70−30)	200	48	134[a]	0	1
	300	174	40	25	35
	400	171	22	29	50
WO_3/CeO_2	200	48	128[a]	0	5
	300	174	35	31	34
	400	171	6	55	39

[a]Additional ammonia is supposed to be produced at this temperature (see text).

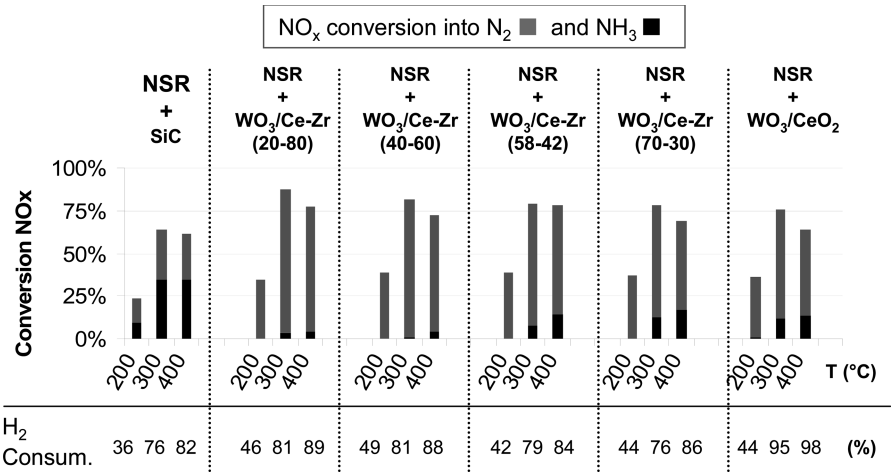

Figure 9. NO_x conversion at 200, 300, and 400 °C over the single NSR (60 mg) catalyst and over the combined NSR + SCR arrangement (NSR/SCR = 60 mg/120 mg). The catalysts were exposed to 500 ppm NO, 10% O_2, 10% H_2O, and 10% CO_2 during the lean period (60 s) and to 3% H_2, 10% H_2O, and 10% CO_2 during the rich period (3 s).

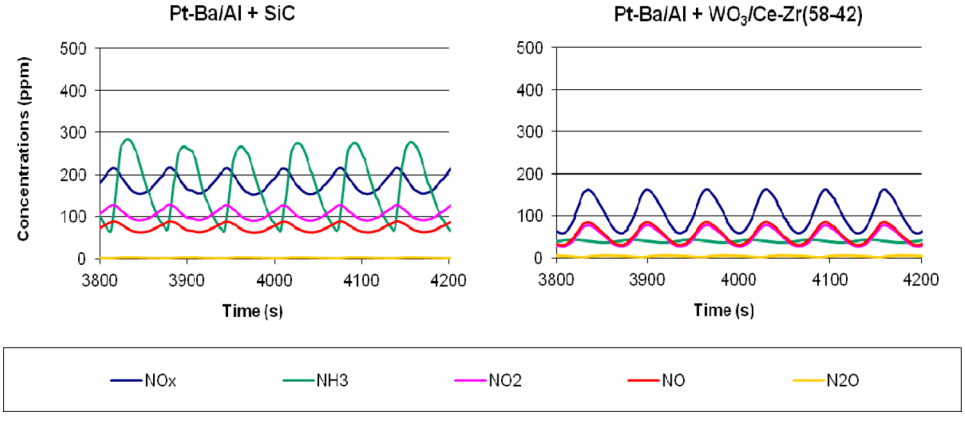

Figure 10. Concentrations of nitrogenous gases obtained by the IR Multigaz analyzer during lean/rich cycling conditions on NSR + SiC and NSR + WO_3/Ce−Zr (58−42); (NSR/SCR = 60 mg/120 mg).

From Table 6, it appears that ammonia is fully used for the additional NO_x conversion at 200 °C. In fact, the additional NO_x conversion is even higher than the quantity of ammonia coming from the NSR catalyst. Then the calculated ratio of ammonia used for the SCR reaction is greater than 100%. This apparent overproduction of ammonia is supported by an overconsumption of H_2 at 200 °C: almost 10% of the introduced hydrogen was consumed, in addition, when WO_3/Ce−Zr materials were added

dx.doi.org/10.1021/cs3008329 | ACS Catal. 2013, 3, 1120−1132

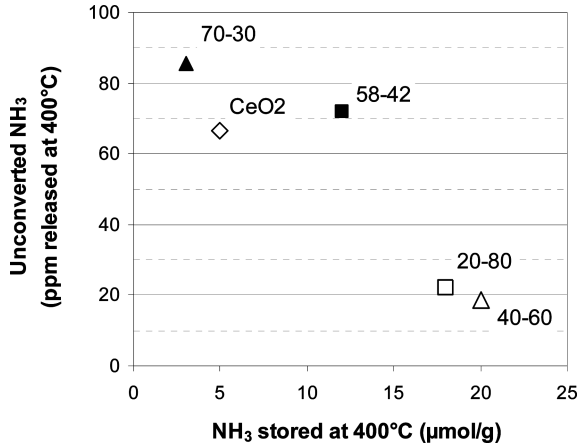

Figure 11. Relationship between unconverted NH_3 at 400 °C (ppm) emitted from NSR + SCR combination catalytic bed and acid sites concentration of NH_3 storage measurement at 400 °C (μmol/g) over WO_3/Ce−Zr-supported catalysts. (◊) CeO_2, (□) 20−80, (△) 40−60, (■) 58−42, and (▲) 70−30.

to the NSR catalyst (Figure 9). At 300 and 400 °C, no significant additional H_2 consumption was observed with the addition of the SCR materials, except for WO_3/CeO_2. This supplementary NH_3 production at 200 °C can be explained by the fact that at this temperature, the formation of isocyanate species may occur during the mixture of the rich and lean fronts where NO, CO_2, and H_2 were present together. Water (10% vol) rapidly hydrolyzed these species, and supplementary ammonia can be formed and then reduce supplementary NO_x.[89] At this temperature, acidity was sufficient to retain all the ammonia emitted from the NSR catalyst (Table 3). WO_3/Ce−Zr materials, which exhibit the higher additional ammonia production, are the most reducible samples with the biggest OSC (WO_3/Ce−Zr (40−60 and 58−42)).

At 300 and 400 °C, in addition to the partial ammonia slip previously discussed, it appears that the ammonia does not exclusively react with NO_x, but does also react with O_2. Figure 12 reports the SCR-to-SCO balance reaction at 300 and 400 °C. Therefore, the optimal NO_x conversion depends on both the amount ammonia that reacts and the selectivity of the used ammonia. For instance, WO_3/Ce−Zr (20−80) is the most active catalyst at 300 °C with the lowest ammonia slip of the evaluated samples: around 75% of the used ammonia reacts with NO_x. For other samples, the NO_x SCR reaction converts only between 50 and 60% of the used ammonia.

At 400 °C, the two more acidic materials (WO_3/Ce−Zr (20−80 and 40−60)) again consumed more ammonia. However, for these two catalysts, only 53% and 36% of the used ammonia, respectively, is converted for the SCR reaction. In contrast, for WO_3/Ce−Zr (58−42), which exhibits an ∼2 times lower ammonia storage capacity at 400 °C (Table 3), the SCR reaction is greatly favored: 83% of the used ammonia reacts with NO_x. In comparison, over WO_3/CeO_2, 90% of the used ammonia is oxidized by O_2 into N_2.

Unfortunately, whatever the temperature tests, there is no clear evidence for a correlation between the SCR/SCO selectivities and one of the studied properties (specific surface area, acidity, apparent E_a, kinetic order, etc.). For instance, WO_3/Ce−Zr (58−42) strongly favors the SCR reaction at 400 °C compared with WO_3/Ce−Zr (40−60), whereas there is no similar difference for these parameters compared with the other samples. However, the oxygen storage capacity at 400 °C could play a major role, since the higher value is observed with WO_3/Ce−Zr (58−42), whereas WO_3/CeO_2 which possessed the lowest OSC, clearly favors the oxidation of ammonia by O_2.

In addition to the SCR/SCO ratio (Figure 12), the comparison of the nitrogenous species (NH_3, NO, NO_2) emitted from the first catalytic bed (NSR catalyst) with those emitted after the NSR + SCR dual bed allows one to discriminate the type of SCR reaction occurring on the WO_3/Ce−Zr catalysts. At 200 °C, the "fast" ($2NH_3 + NO + NO_2 \rightarrow 2N_2 + 3H_2O$) reaction is predominant but the "standard" ($2NH_3 + 2NO + 1/2O_2 \rightarrow 2N_2 + 3H_2O$) reaction also occurs. At higher temperature, only the "fast" NH_3-SCR reaction takes place. From there, it can be assumed that at 300 and 400 °C, only "fast SCR" occurs because of the favorable NO/NO_2 ratio (≈1) obtained after the NSR catalytic bed.[56,90−93]

CONCLUSION

The NO_x reduction in lean−rich cycling conditions was studied comparing two processes: namely, NSR (Pt−Ba/Al) and SCR. First, SCR materials WO_3/Ce−Zr with different Ce−Zr ratios were studied. Addition of well dispersed WO_3 on Ce−Zr induces a loss of (i) the basic properties (NO_x storage capacity), (ii) the oxygen mobility, and (iii) the NO-to-NO_2 oxidation capacity. Addition of tungsten trioxide leads to a significant ammonia storage capacity (acidity) initially not present on the supports, while small changes in the reducibility of materials (H_2-TPR) can be observed. The changes in the acid−base properties by addition of WO_3 on Ce−Zr induce a strong enhancement of catalytic activity in the reaction of NH_3-SCR. All WO_3/Ce−Zr

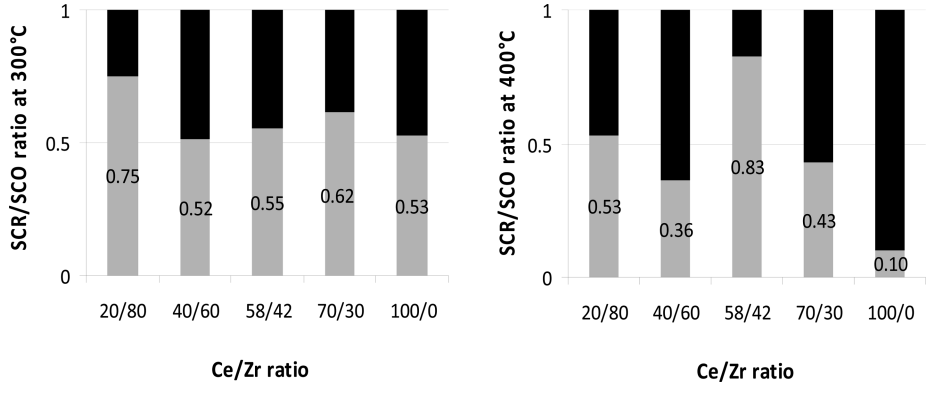

Figure 12. Ammonia used in SCR (gray) to SCO (black) reaction ratio over WO_3/Ce−Zr materials at 300 and 400 °C.

dx.doi.org/10.1021/cs3008329 | ACS Catal. 2013, 3, 1120−1132

materials except WO_3−ZrO_2 become active in NO_x reduction by NH_3 and fully selective in N_2. These solids can reduce more than 80% of NO_x in NH_3-SCR at 350 °C, including CO_2 and H_2O in feed gas. Results suggest that a tetrahedral structure obtained with a 50−50 weight ratio for Ce−Zr promotes NH_3-SCR activity for WO_3/Ce−Zr materials. In the absence of NO_x, a strong oxidation of ammonia by O_2 was also shown, until around 80% of ammonia is oxidized at 500 °C, again exclusively into nitrogen.

Second, these materials were placed downstream from a Pt−Ba/Al model NSR catalyst. Results showed an increase in the quantity of the reduced NO_x in all cases and at all temperatures; however, the acidic properties of WO_3/Ce−Zr do not appear to be strong enough to ensure a total ammonia conversion at high temperature, leading to some ammonia slip. Moreover, from 300 °C, the stored ammonia is not exclusively used for the NO_x−NH_3 reaction; a part also reacts with oxygen. Fortunately, both reactions are fully selective in N_2. Finally, it appears that the SCR reaction occurs following both the standard and fast reaction stoichiometries at 200 °C, whereas only the fast NH_3-SCR occurs at higher temperatures. Finally, these strongly active WO_3/Ce−Zr materials for NO_x reduction by ammonia in nitrogen could be envisaged in the NH_3-SCR process or in addition to a NSR catalyst working in lean−rich cycling conditions.

AUTHOR INFORMATION

Corresponding Author

*Fax: 00 33 (0)549453741. E-mail: fabien.can@univ-poitiers.fr.

Notes

The authors declare no competing financial interest.

REFERENCES

(1) Kobayashi, T.; Yamada, T.; Kayano, K. *SAE Technical Papers 970745*, 1997, *63*.
(2) Elbouazzaoui, S.; Corbos, E. C.; Courtois, X.; Marecot, P.; Duprez, D. *Appl. Catal., B* **2005**, *61*, 236.
(3) Elbouazzaoui, S.; Courtois, X.; Marecot, P.; Duprez, D. *Top. Catal.* **2004**, *30*−*3*, 493.
(4) Konsolakis, M.; Yentekakis, I. V. *J. Catal.* **2001**, *198*, 142.
(5) Shibata, J.; Shimizu, K. I.; Satsuma, A.; Hattori, T. *Appl. Catal., B* **2002**, *37*, 197.
(6) Iliopoulou, E. F.; Evdou, A. P.; Lemonidou, A. A.; Vasalos, I. A. *Appl. Catal., A* **2004**, *274*, 179.
(7) Arve, K.; Klingstedt, F.; Eränen, K.; Wärnä, J.; Lindfors, L. E.; Murzin, D. Yu. *Chem. Eng. J.* **2005**, *107*, 215.
(8) Sobczak, I.; Ziolek, M.; Nowacka, M. *Microporous Mesoporous Mater.* **2005**, *78*, 103.
(9) Chen, S. C.; Kawi, S. *Appl. Catal., B* **2003**, *45*, 63.
(10) Cordoba, L. F.; Sachtler, W. M. H.; De Correa, C. M. *Appl. Catal., B* **2005**, *56*, 269.
(11) Yentekakis, I. V.; Tellou, V.; Botzolaki, G.; Rapakousios, I. A. *Appl. Catal., B* **2005**, *56*, 229.
(12) Maunula, T.; Ahola, J.; Hamada, H. *Appl. Catal., B* **2000**, *26*, 173.
(13) Koebel, M.; Elsener, M.; Kröcher, O.; Schaär, C.; Röthlisberger, R.; Jaussi, F.; Mangold, M. *Top. Catal.* **2004**, *30*−*31*, 43.
(14) Xu, L.; McCabe, R. W.; Hammerle, R. H. *Appl. Catal., B* **2002**, *39*, 51.
(15) Sullivan, J. A.; Doherty, J. A. *Appl. Catal., B* **2005**, *55*, 185.
(16) Flura, A.; Can, F.; Courtois, X.; Royer, S.; Duprez, D. *Appl. Catal., B* **2012**, *126*, 275.
(17) Can, F.; Flura, A.; Courtois, X.; Royer, S.; Blanchard, G.; Marecot, P.; Duprez, D. *Catal. Today.* **2011**, *164*, 474.
(18) Can, F.; Courtois, X.; Royer, S.; Blanchard, G.; Rousseau, S.; Duprez, D. *Catal. Today* **2012**, *197*, 144.
(19) Kinugasa, Y.; Igarashi, K.; Itou, T.; Suzuki, N.; Yaegashi, T.; Tanaka, T. *Device for purifying an exhaust gas of an engine*; U.S. Patent 5782087, July 21, 1998.
(20) Kinugasa, Y.; Itou, T.; Hoshi, K.; Suzuki, N.; Yaegashi, T.; Igarashi, K. *Device for purifying exhaust gas from engine*; U.S. Patent 5964088, October 12, 1999.
(21) Sakurai, K. *Exhaust purifying system for internal combustion engine*; U.S. Patent Appl. 2011/0138783 A1, June 16, 2011.
(22) Sakurai, K.; Miyashita, S.; Katumata, Y. *Exhaust purifying system for internal combustion engine*; U.S. Patent Appl. 2011/0214417 A1, September 8, 2011.
(23) Guenther, J.; Konrad, B.; Krutzsch, B.; Nolte, A.; Voigtlaender, D.; Weibel, M.; Wenninger, G. *Exhaust gas purification process and apparatus with internal generation of ammonia for reducing nitrogen oxide*; U.S. Patent 6338244 B1, January 15, 2002.
(24) Gandhi, H. S.; Cavatalo, J. V.; Hammerle, R. H.; Chen, Y. *Catalyst system for NOx and NH_3 emission*; U.S. Patent Appl. 2004/0076565 A1, April 22, 2004.
(25) Gandhi, H. S.; Cavatalo, J. V.; Hammerle, R. H.; Chen, Y. *Catalyst system for NOx and NH_3 emission*; U.S. Patent 7332135, February 19, 2008.
(26) Li, Y.; Deeba, M.; Dettling, J. C. *Emissions treatment system with NSR and SCR catalysts*; Patent WO 2005/047663 A3, May 26, 2005.
(27) Furbeck, H.; Koermer, G. S.; Moini, A.; Castellano, C. R. *Catalyst, method for its prepration and system to reduce NOx in an exhaust gas stream*; Patent WO 2008/036797 A1, March 27, 2008.
(28) Wan, C. Z.; Zheng, X.; Stiebels, S.; Wendt, C.; Boorse, S. R. *Emissions treatment system with ammonia-generating and SCR catalyst*; Patent WO 2010/114873 A3, October 7, 2010.
(29) Li, Y.; Deeba, M.; Dettling, J. C.; Patchett, J. A.; Roth, S. A. *Emission treatment system with NSR and SCR catalysts*; Patent U.S. 7919051B2, April 5, 2011.
(30) Chen, H. Y.; Weigert, E.; Fedeyko, J.; Cox, J.; Andersen, P. *Advanced Catalysts for Combined (NAC + SCR) Emission Control Systems*; SAE Technical Paper 2010-01-0302.
(31) Hu, H.; Stover, Th. *Hybrid catalyst system for exhaust emissions reduction*; Patent WO 2006/008625 A1, January 26, 2006.
(32) Hu, H.; Stover, Th. *Hybrid catalyst system for exhaust emissions reduction*; U.S. Patent 7213395 B2, May 8, 2007.
(33) Hu, H.; McCarthy, E., Jr.; Yan, Y. *Thermal management of hybrid LNT/SCR aftertreatment during desulfation*; U.S. Patent 7251929 B2, August 7, 2007.
(34) Hu, H.; Stover, Th. *Hybrid catalyst system for exhaust emissions reduction*; U.S. Patent 7650746 B2, January 26, 2010.
(35) McCarthy, E., Jr.; Bailey, O. H. *LNT-SCR system optimized for thermal gradient*; U.S. Patent 7950226 B2, May 31, 2011.
(36) Ginter, D. M.; Mc Carthy, E., Jr. *Optimized rhodium usage in LNT-SCR system*; U.S. Patent 8069654 B2, December 6, 2011.
(37) Lietti, L.; Nova, I.; Forzatti, P. *J. Catal.* **2008**, *257*, 270.
(38) Koebel, M.; Madia, G.; Elsener, M. *Catal. Today* **2002**, *73*, 239.
(39) Nova, I.; Ciardelli, C.; Tronconi, E.; Chatterjee, D.; Bandl-Konrad, B. *Catal. Today* **2006**, *114*, 3.
(40) Forzatti, P.; Lietti, L.; Tronconi, E. In *Nitrogen Oxides Removal—Industrial. Encyclopaedia of Catalysis*, 1st ed.; Horvath, I. T., Ed.; Wiley: New York, 2002, and references therein.
(41) Kato, A.; Matsuda, S.; Kamo, T.; Nakajima, F.; Kuroda, H.; Narita, T. *J. Phys. Chem.* **1981**, *85*, 4099.
(42) Bosch, H.; Janssen, F. *Catal. Today* **1988**, *2*, 369.
(43) Apostolescu, N.; Geiger, B.; Hizbullah, K.; Jan, M. T.; Kureti, S.; Reichert, D.; Schott, F.; Weisweiler, W. *Appl. Catal., B* **2006**, *62*, 104.
(44) Qi, G. S.; Yang, R. T.; Chang, R. *Appl. Catal., B* **2004**, *51*, 93.
(45) Krishna, K.; Seijger, G. B. F.; Van den Bleek, C. M.; Calis, H. P. A. *Chem. Commun.* **2002**, 2030.
(46) Long, R. Q.; Yang, R. T. *J. Catal.* **1999**, *188*, 332.
(47) Ma, A. Z.; Grunert, W. *Chem. Commun.* **1999**, 71.
(48) Carja, G.; Delahay, G.; Signorile, C.; Coq, B. *Chem. Commun.* **2004**, 1404.
(49) Verdier, S.; Rohart, E.; Bradshaw, H.; Harris, D. *SAE Technical Paper 2008-01-1022* **2008**, DOI: 10.4271/2008-01-1022.

(50) Rohart, E.; Kröcher, O.; Casapu, M.; Marques, R.; Harris, D.; Jones, C. *SAE Technical Paper 2011-01-1327* **2011**, DOI: 10.4271/2011-01-1327.
(51) Li, Y.; Cheng, H.; Li, D.; Qin, Y.; Xie, Y.; Wang, S. *Chem. Commun.* **2008**, 1470.
(52) Chen, L.; Li, J.; Ge, M.; Zhu, R. *Catal. Today* **2010**, *153*, 77.
(53) Lietti, L. *Appl. Catal., B* **1996**, *10*, 281.
(54) Corbos, E. C.; Courtois, X.; Can, F.; Marécot, P.; Duprez, D. *Appl. Catal., B* **2008**, *84*, 514.
(55) Le Phuc, N.; Courtois, X.; Can, F.; Berland, S.; Royer, S.; Marecot, P.; Duprez, D. *Catal. Today* **2011**, *176*, 424.
(56) Masdrag, L.; Courtois, X.; Can, F.; Duprez, D. *Appl. Catal., B* submitted.
(57) Kacimi, S.; Barbier, J., Jr.; Taha, R.; Duprez, D. *Catal. Lett.* **1993**, *22*, 343.
(58) Damyanova, S.; Perez, A.; Schmal, M.; Bueno, J. M. C. *Appl. Catal., A* **2002**, *234*, 271.
(59) Yao, M. H.; Baird, R. J.; Kunz, F. W.; Hoost, T. E. *J. Catal.* **1997**, *166*, 67.
(60) Rossignol, S.; Gerard, F.; Duprez, D. *J. Mater. Chem.* **1999**, *9*, 1615.
(61) Li, X. W.; Shen, M. M.; Xi, H.; Zhu, H. Y.; Gao, F.; Yan, K.; lin, D.; Yi, C. *J. Phys. Chem. B.* **2005**, *109*, 3949.
(62) Lê, P. N.; Corbos, E. C.; Courtois, X.; Can, F.; Royer, S.; Marecot, P.; Duprez, D. *Top. Catal.* **2009**, *52* (13−20), 1771.
(63) Parry, E. P. *J. Catal.* **1963**, *2*, 371.
(64) Trietyakov, N. E.; Filimonov, V. N. *Kinet. Katal.* **1973**, *14*, 803.
(65) Knözinger, H. *Adv. Catal.* **1976**, *25*, 184.
(66) Larsen, G.; Lotero, E.; Raghavan, S.; Parra, R. D.; Querini, C. A. *Appl. Catal., A* **1996**, *139*, 201.
(67) Abbattista, F.; Delmastro, S.; Gozzelino, G.; Mazza, D.; Vallino, M.; Busca, G.; Lorenzelli, V.; Ramis, G. *J. Catal.* **1989**, *117*, 42.
(68) Tamura, M.; Shimizu, K. I.; Satsuma, A. *Appl. Catal., A* **2012**, *433−434*, 135.
(69) Zaki, M. I.; Hasan, M. A.; Al-Sagheer, F. A.; Pasupulety, L. *Coll. Surf. A.* **2001**, *190*, 261.
(70) Hussein, G. A. M.; Gates, B. C. *J. Catal.* **1998**, *176*, 395.
(71) Hussein, G. A. M.; Gates, B. C. *J. Chem. Soc., Faraday Trans.* **1996**, *93*, 2425.
(72) Connel, G.; Dumesic, J. A. *J. Catal.* **1986**, *101*, 103.
(73) Nakano, Y.; Iizuka, T.; Hattori, H.; Tanabe, K. *J. Catal.* **1979**, *57*, 1.
(74) Kourieh, R.; Bennici, S.; Marzo, M.; Gervasini, A.; Auroux, A. *Catal. Comm.* **2012**, *19*, 119.
(75) Triwahyono, S.; Yamada, T.; Hattori, H. *Appl. Catal., A* **2003**, *242*, 101.
(76) Zaki, M. I.; Hussein, G. A. M.; Mansour, S. A.; El-Ammay, H. A. *J. Mol. Catal.* **1989**, *51*, 209.
(77) Le, P. N.; Corbos, E. C.; Courtois, X.; Can, F.; Marecot, P.; Duprez, D. *Appl. Catal., B* **2009**, *93*, 12.
(78) Reiche, M. A.; Maciejewski, M.; Baiker, A. *Catal. Today* **2000**, *56*, 347.
(79) Vermaire, D. C.; Van Berge, P. C. *J. Catal.* **1989**, *116*, 309.
(80) Wilken, N.; Wijayanti, K.; Kamasamudram, K.; Currier, N. W.; Vedaiyan, R.; Yezerets, A.; Olsson, L. *Appl. Catal., B* **2012**, *111−112*, 58.
(81) Brandenberger, S.; Kröcher, O.; Wokaun, A.; Tissler, A.; Althoff, R. *J. Catal.* **2009**, *268*, 297.
(82) Kustov, A. L.; Hansen, T. W.; Kustova, M.; Christensen, C. H. *Appl. Catal., B* **2007**, *76*, 311.
(83) Shan, W.; Liu, F.; He, H.; Shi, X.; Zhang, C. *Appl. Catal., B* **2012**, *115−116*, 100.
(84) Shan, W.; Liu, F.; He, H.; Shi, X.; Zhang, C. *Chem. Commun.* **2011**, *47*, 8046.
(85) Luo, J. Y.; Hou, X.; Wijayakoon, P.; Schmieg, S. J.; Li, W.; Epling, W. S. *Appl. Catal., B* **2011**, *102*, 110.
(86) Ozkan, U. S.; Cai, Y.; Kumthekar, M. W. *J. Catal.* **1994**, *149*, 390.
(87) Ramis, G.; Busca, G.; Bregani, F.; Forzatti, P. *Appl. Catal.* **1990**, *64*, 259.
(88) Brandenberger, S.; Kröcher, O.; Tissler, A.; Althoff, R. *Catal. Rev.* **2008**, *50*, 492.
(89) Corbos, E. C.; Haneda, M.; Courtois, X.; Marecot, P.; Duprez, D.; Hamada, H. *Catal. Comm.* **2008**, *10*, 137.
(90) Koebel, M.; Elsener, M.; Madia, G. *Ind. Eng. Chem. Res.* **2001**, *40*, 52.
(91) Koebel, M.; Madia, G.; Elsener, M. *Catal. Today* **2002**, *73*, 239.
(92) Yeom, Y. H.; Henao, J. J.; Li, M. J.; Sachtler, W. M. H.; Weitz, E. *J. Catal.* **2005**, *231*, 181.
(93) Ciardellia, C.; Nova, I.; Tronconia, E.; Chatterjee, D.; Burkhardt, T.; Weibel, M. *Chem. Eng. Sci.* **2007**, *62*, 5001.